Flows, transport, and form drag in intertidal salt marsh creeks

Collin J. Ortals[1], Orlando Cordero[2], Arnoldo Valle-Levinson[1], Christine Angelini[1,3]

[1]Department of Civil and Coastal Engineering, University of Florida, Gainesville, FL, USA, [2]Department of Geological Sciences, University of Florida, Gainesville, FL, USA, [3]Department of Environmental Engineering Sciences, University of Florida, Gainesville, FL, USA

Corresponding author: Collin Ortals (collin.ortals@ufl.edu)

Key Points:

- Form drag is ~3-12 times greater than bed drag in intertidal creeks with channel widths less than 5 meters.
- Within a confined drainage area, multiple creeks have opposing tidal asymmetries with respect to peak velocity, tidal transport, and total suspended solids (TSS) transport.
- Net circulations on marsh platform during intermediate and spring tides suggest that tidal creek flows regularly exchange and interact with one another.
- Opposing creek asymmetries and platform circulations have the potential to lead to heterogeneity in marsh geomorphic evolution and response to sea level rise.

Abstract

Intertidal creeks (<5m width) weave through salt marshes, delivering water, nutrients, and sediments into the marsh interior and alter spatial heterogeneity in plant and animal distributions. Despite their global prevalence, creek connectivity, and the mechanisms controlling cross-marsh hydrodynamics, remain poorly resolved. In this study, we measured flow and total suspended solids (TSS) transport in three intertidal creeks within a confined drainage basin in a Georgia, USA salt marsh. We discovered that the effective drag is 3 to 12 times greater than bed drag, reaching levels similar to those observed in coral reefs. Furthermore, the drag between tidal flood and ebb phases differ, suggesting a non-symmetric drag. Analyses of along-channel momentum reveal that the friction $O(10^{-3} - 10^{-2})$ and pressure gradient $O(10^{-3} - 10^{-2})$ dominate creek momentum balance. Divergence in tidal and TSS transport between adjacent creeks reveals opposing tidal asymmetries within this confined basin. We suggest that these differences may mediate the eco-geospatial evolution of salt marshes and their response to sea level rise.

Plain Language Summary

Salt marshes generate a valuable suite of ecological and economic services. Key to understanding their fate in relation to rising sea levels is understanding eco-physical dynamics of the creeks that weave through these marshes, as these features serve as major conduits of water, sediments, and biological material exchange. Models have been developed to explain how flow moves through creeks over one tidal cycle. However, there are limited field measurements resolving the dominant forms of drag controlling tidal fluxes through creeks, divergences in water flow and sediment transport between creeks, or creek-creek circulations. This study applies field measurements from a Georgia salt marsh to address these knowledge gaps. We discover that adjacent creeks in a confined drainage basin are governed by form drag produced by flow interactions with the landscape and vegetation and exhibit profound heterogeneity in tidal flows and sediment transport. We highlight that this local-scale heterogeneity likely plays a major role in mediating the pattern and mechanisms by which salt marshes are responding to sea level rise.

1 Introduction

1.1 Salt marshes and tidal creeks

Salt marshes form along temperate, low-energy coastlines worldwide where they provide valuable ecological (e.g. C-sequestration, N-cycling, biodiversity enhancement) and economic services (e.g. fisheries, storm surge reduction) (Barbier et al., 2011; Bouma et al., 2014; Temmerman et al., 2013). These tidally flooded landforms are created via sedimentation, a process which is enhanced by vegetation (Fagherazzi et al., 2012). The feedbacks that occur between water flow, vegetation and sedimentation allow salt marshes to adjust in vertical relief and spatial extent in response to sea level changes and shorter timescale events – such as hurricanes, droughts, and oil spills (Coverdale et al., 2012; Fagherazzi et al., 2012; Lin & Mendelssohn, 2012). Within these biogenic coastal landforms, tidal channels and creeks bisect elevated marsh platforms, forming networks that control the exchange of water (Bayliss-Smith et al., 1979; Boon, 1975; French & Stoddart, 1992; Healey et al., 1981; Hughes, 2012; Mariotti & Fagherazzi, 2011), sediments (Christiansen et al., 2000; Voulgaris & Meyers, 2004), and suspended biological material between the estuary and marsh interior (Struyf et al., 2013).

Previous research has focused on understanding water flow and sediment transport in subtidal channels with widths between 10s and 1000s of meters. However, few studies have measured or analyzed flows in intertidal creeks with widths smaller than 10s of meters. This is despite the ubiquity of intertidal creeks in salt marshes and their propensity to modify flow and sedimentation patterns, and control the fitness and distribution of plants and animals across marsh landscapes (Pieterse et al., 2012, 2015).

In this paper, field measurements are analyzed to address three gaps in the literature related to intertidal creek (<10 m wide) flows and sediment transport: 1) what are the velocities in multiple tidal creeks in a confined drainage basin? 2) What are the sources and effects of tidal creek drag? and 3) What are the mechanisms underlying creek connectivity and cross-marsh circulations, and how do they depend on tidal phase? We summarize these knowledge gaps in the sections below and focus our field measurements in a Georgia (USA) salt marsh.

1.2 Velocities in multiple tidal creeks in a confined drainage basin

A simplified model (Boon et al., (1975) explained the tidal stage-velocity (discharge) asymmetry [differences in velocity (discharge) at the same tidal stage for different phases of the tide] in a tidal creek. While this model helped explain general patterns in tidal asymmetry, it could not fully reproduce the tidal asymmetries, and in particular, the surge effect on ebb tides at below-bank elevations, or when outflow concentrates through the channel rather than overbank flow (Fagherazzi et al., 2008a). This was due to key limiting assumptions, namely that the model did not consider wind stresses and assumed that: (1) the water surface is ‘flat’ (no water level slopes), (2) the system is frictionless (i.e., water disperses through system instantaneously), and (3) all flow passes through the channel section (i.e., no overbank flow). Subsequent studies identified the need to expand the study area to include the role of overbank flow (French & Stoddart, 1992), a process that Temmerman et al. (2005) determined could account for 0-60% of the water budget in a marsh, depending on the tidal amplitude and environmental conditions, such as wind forcing. Fagherazzi et al. (2008a) expanded the Boon model by incorporating a constant linearized friction term on the landscape, whereby water surface elevation gradients on the marsh are estimated through Poisson’s Equation which are a function of average water depth, the friction coefficient, and change in stage of the tidal inlet. Furthermore, time-varying infilling and outflowing was accounted for by estimating travel time distributions in both channels and on the marsh platforms. Their model was able to capture the time-lagging effects of tidal asymmetries previously uncaptured by the Boon model. Importantly, the data used to validate these models were limited to field measurements of a single creek and thus, it is unclear if they are able to resolve potential interactions between multiple adjacent creeks.

1.3 Sources and effects of tidal creek drag

Frictional drag is caused by different features in coastal landscapes, including bed material (Grant & Madsen, 1982; Nikuradse, 1933), topographical elements (Monismith, 2007; Warner & MacCready, 2014), channel structure (Bo & Ralston, 2020; Kranenburg et al., 2019; Li et al., 2004), and vegetation (Monismith et al., 2019; Nepf, 1999). Frictional drag has been characterized in various forms such as friction factors (i.e. Darcy-Weisbach) or coefficients (i.e. Manning’s n) (Yen, 2002) or non-dimensional quadratic drag coefficients (Bo & Ralston, 2020). A source of drag in marsh landscapes can be bottom drag, which results from fluid flow and bed interactions that form a boundary layer at the interface. These interactions result in the characteristic logarithmic velocity profiles for fluids: (Equation 1),

$$u(z) = \frac{u_*}{\kappa}\left[\ln\left(\frac{z-d}{z_0}\right)\right] + \beta \tag{1}$$

whereby the magnitude of bed drag generally scales with the bed roughness height z_0 (Nikuradse, 1933) or with the size of bedforms (Grant & Madsen, 1982). In Equation 1, $u(z)$ is the fluid velocity at reference height z above the bed, κ is the von Karman's constant ($= 0.41$), u_* is the shear velocity at z, d is the local water depth, and β is a correction coefficient. Bottom drag is often expressed in terms of a dimensionless coefficient, $C_{d,bot}$ (Voulgaris & Meyers, 2004) and can be related to the bottom roughness height using:

$$z_o = z\,exp(-\kappa/(C_{d,bot})^{\frac{1}{2}}) \tag{2}$$

Note that the bottom drag coefficient is typically referred to as C_d in literature, however, in this work it is referenced as $C_{d,bot}$ to distinguish from other types of drag considered. The bed drag coefficient can be solved for using the following relationships:

$$\tau = \rho(C_{d,bot})u_{*,bot}^2 \tag{3}$$

$$\tau = \rho u_z^2 \tag{4}$$

Where τ is the bed shear stress and u_z is the reference streamwise velocity.

Additionally, drag can be evaluated in terms of effective, or form drag, caused by different features in the landscape, such as vegetation or reefs. This is often expressed in the form of the dimensionless drag coefficient, $C_{d,eff}$, which is the ratio between inertial and pressure gradient terms with friction terms in the momentum equation (Kranenburg et al., 2019; Li et al., 2004; Monismith, 2007). In controlled laboratory settings, the drag effects from various features (e.g., vegetation) can be isolated (Nepf, 1999). In field settings, however, it is infeasible to isolate the different contributing factors (i.e. vegetation, bed, microtopography effects). Therefore, it is useful to express drag as a bulk term, or the 'integrated effects' of the landscape (Monismith et al., 2019). Efforts have been made to estimate the drag effects from reefs which have been found to be up to 10x greater than the canonical 0.0025 value for muddy or sandy sea beds (Monismith, 2007). Furthermore Monismith et al. (2019) found that the drag from seagrass beds can range from 0.05 to 1 depending on the phase of the tide.

In this study, $C_{d,eff}$ is reported as a function of water level at two intertidal salt marsh creeks. The study also describes the importance of effective drag relative to bed drag in these systems. Understanding their relative importance is necessary for resolving the controlling mechanisms in salt marsh creeks as well as to understanding how vegetation and other form features may modulate flow during different stages of the tide.

1.4 Creek-to-creek flow interactions and overmarsh circulations

Building upon enhanced understanding of flows that occur near the marsh-channel interface, Torres et al. (2007) conducted a field campaign to quantify overmarsh circulation and creek flows. Their study revealed that regular exchanges of water occur at the heads of tidal creeks (i.e. where tidal creeks terminate in marsh platforms) and suggested that drainage basins, or divides, are not clearly or consistently delineated during high water events within salt marshes, a pattern contrary to well-defined, temporally stable divides in fluvial systems. Using numerical simulations of marsh circulation in which first and second order tidal creeks were systematically removed from a high resolution digital elevation model (resulting in a <60% reduction of drainage density), Sullivan et al. (2019) discovered that such creek removal did not affect large-scale circulation and tracer dispersal. However, following the removal of third and fourth order creeks as well (an up to 85% reduction of drainage density), the authors discovered that the system transitioned from being ebb- to flood-dominated. This change was caused by losses in hydraulic conductivity and the ability of tidal creeks to convey water further into the marsh platform interior. While small intertidal creeks may not control km-scale overmarsh circulations, it is unclear whether creek-creek flow interactions lead to limited inflow or early flow reversals of adjacent creeks. Creek dynamics have the potential to alter tidewater resonance time, sedimentation, and the exchange of biological material.

2 Materials and Methods

2.1 Field site characteristics

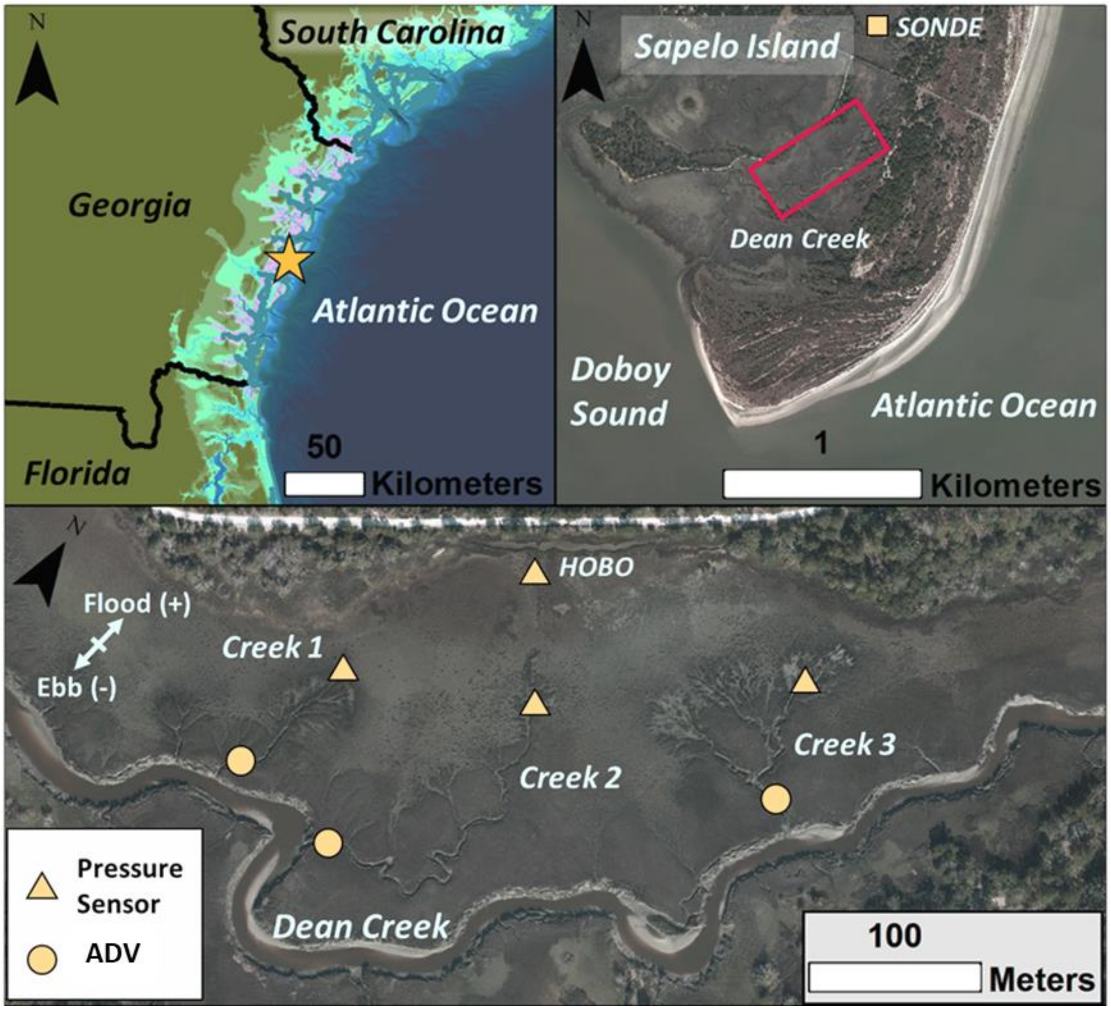

Figure 1. Overview of study site, including the location of Sapelo Island (star) within the South Atlantic Bight (a), the Dean Creek marsh-creek system on the southern end of Sapelo Island (b), and the location of our field study area, deployed instruments (pressure sensors highlighted as yellow triangles, and Vectors (ADVs) as yellow circles), and naming convention for creeks referred to throughout the paper (c). Note that the dataframe in (c) is rotated from north (as denoted in red box Panel b).

To address these three knowledge gaps, we conducted a field study on Sapelo Island, Georgia, USA, within the South Atlantic Bight (SAB) (Figure 1A), a region which is dominated by semi-diurnal tides. The tidal amplitude in this area ranges from ~0.5 to 1.6 m over the spring-neap tidal period. The coastal region in this area is characterized by barrier islands and intertidal wetlands (ranging from freshwater, brackish, and salty) along the estuarine gradient fed by major tributaries, namely the Ogeechee River, Blackbeard Creek, Altamaha River, and Satilla River. At our site, the salt marsh is dominated by monocultures of *Spartina alterniflora*, a C4 grass that ranges in height from 0.3-0.5 m in higher-elevation marsh platforms to > 2 m in height along lower elevation creek banks. Our site, a marsh area fed by Dean Creek on the southern tip of Sapelo Island (Figure 1 b/c), is located within the Sapelo Island National Estuarine Research Reserve (SINERR), which operates long-term ecological and hydrological monitoring stations as a part of the U.S. NERR System-Wide Monitoring Program.

Dean Creek and its surrounding intertidal salt marshes are bordered to the east by an upland forested relic dune system (driven by island migration), to the north by a road and bridge leading to the beach, and to the west by another road built along a formerly hummocked upland strip of land. The southern end of Dean Creek is connected to the Doboy Sound, near to the Atlantic Ocean (roughly 1.2 km inland). The focal marsh area is approximately 0.52 km^2 (52.3 hectares). The segment of Dean Creek in our domain is approximately 2.1 km long and, on average, approximately 20 meters wide, and has an average sinuosity ($= \frac{total\ creek\ length}{creek\ straight{-}line\ length}$) of 1.5. Our study site (outlined in red Figure 1b) is 1 km to 1.5 km upstream of the confluence between Dean Creek and the Doboy Sound.

The focal drainage basin (0.07 km^2 or 7.45 hectares in area) at our study site (Figure 1c, note that map is rotated from north), is primarily fed by three intertidal creeks (channel widths < 5 m), herein referred to by their naming convention – Creek 1, 2 and 3 - labeled in the map. The creekmouth bed elevation of each creek is approximately -0.57, -0.53, and -0.94 meters above mean sea level (m.a.m.s.l.), respectively. Details regarding each creeks' geomorphic characteristics are in Table 1. The low marsh elevation varies from ~0.6-0.8 m.a.m.s.l. at the site, with higher levees along Dean Creek's channel banks reaching elevations of 1.15 m.a.m.s.l., a level equivalent to the local mean higher high water – MHHW.

Table 1

Creek Characteristics (2006-2016)

Creek ID	Type	*L (m)*	*S*	*ΔL (m/y)*	*% change L*	Confluence location***	Confluence orientation***
Creek 1	Single Threaded	100	1.1	2	25	straight-away	normal
Creek 2	Single Threaded	270	1.7	0.5	2	bend apex**	coincident
Creek 3	Reticulated	130*	---	1.4	---	straight-away	normal

*Longest reticulated segment
**Main Channel bend (*W/R*) = 0.8
***Relative to main channel

2.2 Field instrumentation

We deployed one Nortek Vector acoustic Doppler velocimeter (ADV) in each of three adjacent tidal creeks within a contiguous salt marsh fed by Dean Creek on Sapelo Island, Georgia (31°23'22.88"N, 81°16'29.07"W, see Fig. 1 for map of instrument array and tidal creek naming convention). Each ADV was deployed 5-10 m upstream of each creek mouth by mounting the instrument to a steel frame that included a crossbar that spanned the tidal creek; a bubble level was used to ensure the ADVs were mounted vertically with the sensors facing down. Sampling volumes were 20, 30, and 30 cm above the bed for Creeks 1, 2 and 3, respectively. We paired each ADV with an RBR SoloD Fast8 pressure sensor (herein referred to as pressure sensor) which was positioned upstream of each ADV. The streamwise distances between each ADV and its paired pressure sensor were 85, 220, and 110 m for Creeks 1, 2 and 3, respectively. The pressure sensors were mounted to a metal t-post which was driven into the marsh until resistance was met. A HOBO pressure sensor was mounted adjacent to Lighthouse Road in air, approximately 2.5 m.a.s.l., to capture the local atmospheric pressure variations. All instrument positions were surveyed to UTM 17N coordinate system and the local mean sea level vertical datum with a Trimble Geo7x RTK-GPS. The ADVs were set to record in continuous, pulse-coherent mode at 32 Hz for the duration of the experiment. The pressure sensors were set to 8 Hz, and the HOBO was set to 1 Hz. All data recordings when the instruments were not submerged during low tide were discarded. A total of 20 tidal cycles were captured for all instruments. The start and end dates of the study were July 25, 2019 to August 5, 2019, which is during peak productivity periods of *Spartina alterniflora*.

2.3 Data post-processing

2.3.1 Water levels

Water levels for ADVs and pressure sensors were computed by subtracting out the local atmospheric pressure (measured with HOBO), converting to water depth, and then adding the reference elevation value taken with an RTK. To assess the along channel pressure (water surface) slopes, we made small vertical adjustments in each pressure sensor and computed water level such that the gradient would be zero when the ADV measured zero flow (due to small vertical errors in survey equipment measurements, < 3 cm). Then we used Creek 2 water level as our fixed reference and assumed that, at high water measured for each pressure sensor (marsh platform), each sensor would have the same peak water surface elevation. The precision for pressure measurements is 0.01 dbar for the RBRs and 0.01 dbar for the ADVs, which translates to ~1 cm accuracy in depth.

2.3.2 ADVs

A low signal-to-noise ratio (SNR) in pulse-coherent acoustic instruments, or the ratio of instrument signal intensity compared to the instrument background noise level, can be caused by low amounts of particles, or ‘scatterers’, in the water column (Voulgaris & Trowbridge, 1998). In marsh systems, this can occur during slack tide when water velocities are slow or close to zero, and particles have had time to settle in the water column. As recommended by the manufacturer for Nortek Vectors (Rusello, 2009), we applied a cutoff of 30 SNR where velocity measurements below the threshold were removed and replaced with a 5-minute windowed mean value (i.e. averaged 2.5 minutes prior and 2.5 minutes post replacement measurement).

Another issue with pulse-coherent recording mode can arise with signal phase-wrapping (Rennie & Hay, 2010). Phase wrapping occurs when the *in-situ* velocities exceed the so-called ambiguity velocity, or maximum beam velocity that can be measured in its given configuration. Velocities in ADVs are determined by measuring the Doppler phase shift between emitted and returned acoustic pulses. The measurable velocity range (ambiguity) is scaled between –π and +π and, if this is exceeded, a phase-wrap occurs (Rusello, 2009). The ambiguity velocity equation is $V_{amb} = c/(4fL)$ where c is the speed of sound in water [m/s], f is the internal instrument frequency [Hz], and L is the time lag, an intrinsic property of the instrument [s]. This is sometimes difficult to avoid in the field as *a priori* knowledge of the expected velocities is needed. Setting the instrument velocity range too high can introduce undesired noise in the signal and reduce data quality. (Goring & Nikora, 2002) suggested to replace a velocity spike with either the local mean value or use a 12-point cubic spline. As the cubic spline produced large values, we used a local mean value. The spikes were identified using the phase-space method (Goring & Nikora, 2002) and a 5 minute window, or N=9,600 samples. After accounting for the phase-wrapping, we rotated the velocity measurements to represent the streamwise (u), cross-stream (v), and vertical (w) axes for each channel. Positive (+) streamwise values in subsequent analyses represents flooding and negative (-) represents ebbing.

2.3.3 Estimating bottom and effective drag coefficients

ADVs have successfully been used to estimate quadratic bottom drag coefficient in various coastal and estuarine environments including in estuaries with mud flats, tidal channels, and the wave breaking zone (Blanton et al., 2004; Feddersen et al., 2003; Nidzieko & Ralston, 2012; Voulgaris & Meyers, 2004). The bottom drag coefficient $C_{d,bot}$ depends on the bottom roughness height z_0 (Nikuradse, 1933) or bedforms (Grant & Madsen, 1982) (Equations 1-3). This is a key parameter in understanding vertical variation in velocity, or the shear stresses, which are important for bed erosion. ADVs have been found to accurately measure turbulent velocity fluctuations, where the cross-correlation of the horizontal and vertical components can predict the shear velocity in the Reynolds Stress Method (Soulsby, 1983) (Equations 5-6).

$$u_{*,z} = (\langle u'w' \rangle^2 + \langle v'w' \rangle^2)^{1/4} \tag{5}$$

$$u{*_{bot}}^2 = \frac{{u_{*,z}}^2}{1 - \frac{z}{d}} \tag{6}$$

where $u_{*,z}$ is the shear velocity at elevation z above the bed, u', v', and w' are the deviations from a time average velocity denoted by brackets and representing 10-min data sets, and d is the local water depth. The drag can then be estimated as the best fit line of data where $C_{d,bot} = {u_{*,bot}}^2/{u_z}^2$. In addition, the effective drag (form + bottom drag) allows understanding on how the integrated effects of bathymetry (e.g. (Monismith, 2007; Warner & MacCready, 2014) or vegetation (e.g. (Monismith et al., 2019; Nepf, 1999)) alter water flow and sediment transport. Effective drag values for tidal creeks of this size (channel width <5 m) have not yet been estimated from field measurements. Values were assessed at each ADV location. We assume that water density is spatially constant in our study site, thus neglecting baroclinicity. We then used a one-dimensional streamwise x momentum equation:

$$\frac{\partial U}{\partial t} + U\frac{\partial U}{dx} = -g\frac{\partial \eta}{\partial x} - C_{d,eff}\frac{U\,U}{R_h} \tag{7}$$

where U is the cross-sectionally averaged streamwise velocity, x is the along-channel distance, η is the water surface elevation, and R_h is the hydraulic radius (section flow area A over the section wetted perimeter P). Due to instrument limitations, we replace U with u_z, the locally measured velocity, as we could not resolve the cross channel velocity structure with our instrument array. From scaling, the inertial terms (terms on the left-hand side of eq. 7) are assumed to be small (i.e.

time and length scales are much greater than the velocity) (Friedrichs & Madsen, 1992; LeBlond, 1978). Since the channel width is the same order of magnitude as the water depth, the hydraulic radius cannot be approximated as the water depth. Solving for $C_{d,eff}$, we have the following relationship:

$$C_{d,eff} = \frac{-g\frac{\Delta\eta}{\Delta x}}{\frac{u_z u_z}{R_h}} \tag{8}$$

where $\frac{\Delta\eta}{\Delta x}$ is the along channel water surface gradient, computed with the RBR and ADV pressure measurements, and R_h is solved iteratively for different water depths using RTK survey measurements. The ratio of effective and bed drag, $C_{d,eff}/C_{d,bot}$, represents the proportion of total drag relative to bed drag which reduces to the following relationship:

$$\frac{C_{d,eff}}{C_{d,bot}} = g\frac{A}{P}\frac{\Delta\eta/\Delta x}{{u_*}^2} \tag{9}$$

which indicates that as the water depth approaches 0 then $C_{d,eff}/C_{d,bot} \rightarrow 1$ meaning the total drag is due to the bed. If $C_{d,eff}/C_{d,bot} \gg 1$, it indicates that drag from other sources dominates the frictional effects.

2.3.4 Tidal and TSS Transport

Tidal exchange and TSS transport were estimated for each creek and for each tidal cycle. The tidal exchange is approximated in each channel by first estimating the mean streamwise velocity using the von Karman-Prandtl equation (Equation 1) by subdividing the profile over N=50 vertical sigma layers (function of water depth at time t) (Dyer, 1971). z_0 was estimated by solving the following equation, $z_0 = z \times \exp(-\kappa/(C_{d,bot})^{1/2})$ (Voulgaris & Meyers, 2004). Previous authors have suggested using a two-point method for fitting a logarithmic profile, i.e. ADV or current meter placed at 0.2d above bed and 0.8d above bed where d is the total water depth [m] and then averaged (Walker, 1988). Due to instrument availability, we utilized one instrument for each location and estimated the vertical velocity profile, and used the 0.6d (d = depth at time of measurement) velocity to be representative of the section (Rantz, 1982; Walker, 1988). To understand the uncertainty in estimating the section average discharge, we incorporated a factor of uncertainty to the mean velocity estimate (i.e. an increase or decrease of 33%) which can be seen in Figure 6. In addition, part of the tidal cycle is not captured due to instrument drying at lower tidal elevations. We consider this not to be a shortcoming, however, because the main purpose of this study is to understand directionality of exchange (either net flood, net ebb, or neutral), rather than establish a budget.

To estimate the total suspended sediments (TSS) in each creek, we collected water samples using bilge pumps mounted to t-posts at the same elevation as the ADV sampling volume and approximately 1 meter upstream from each ADV. Samples were taken at 30-minute intervals for 5 hours over the course of one tidal cycle. All samples were kept on ice until transported to the lab, where they were filtered through Whatman Glass Fiber Filters (0.7µm) and freeze dried to remove moisture. Filter pre-weights were subtracted from post-weights and divided by the volume of water filtered for each sample. TSS exchanges were estimated by multiplying the concentration values and estimated tidal discharge. Measured TSS values ranged from 24 to 140 mg/L in our datasets (see supplemental data).

For subsequent analyses, we interpreted our data in three groupings based on tidal amplitude relative to approximate tidal creek bank elevation (0.8 m.a.m.s.l.) and MHHW estimated from the nearby NOAA Rockdedundy harmonic tidal prediction station (1.15 m.a.m.s.l.). For brevity, the zones are hereafter referred to as Neap (< 0.8 m.a.m.s.l.), Intermediate (> 0.8 m.a.m.s.l. and < 1.15 m.a.m.s.l.), and Spring Tides (> 1.15 m.a.m.s.l.). In addition, to compare across creeks, tidal times presented in subsequent figures are relative to Creek 2 high water as the three creeks experience high water at different times.

4 Results

4.1 Stage-Velocity Relationships at Creekmouths

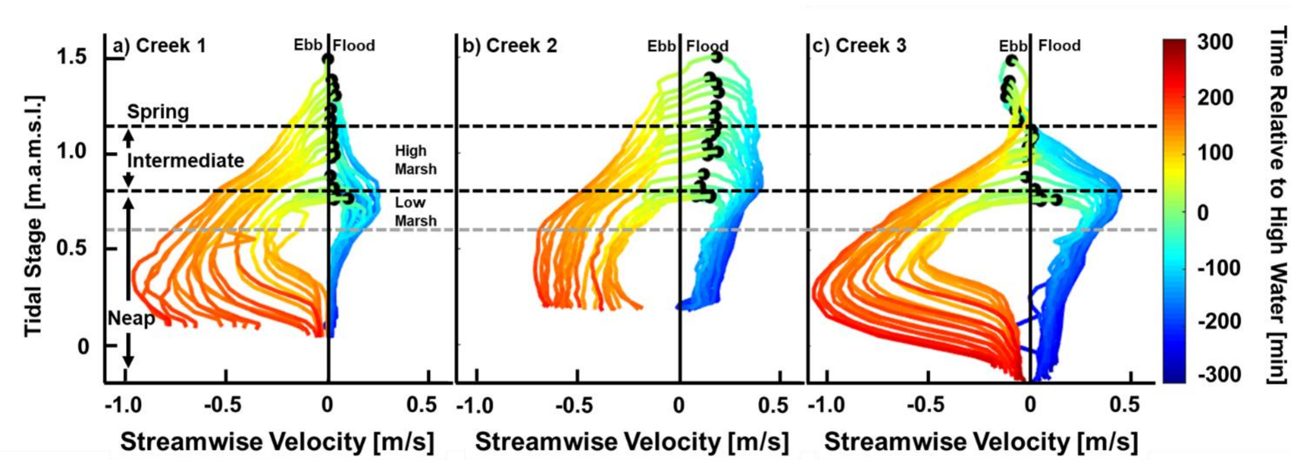

Figure 2. The stage-velocity (streamwise component) relationship for all available data from ADVs in Creeks 1 (a), 2 (b), and 3 (c). Positive velocity values indicate tidal flooding and negative indicate ebbing. The colors indicate time (min) relative to Creek 2 high water [(-) is prior and (+) is after high water]. Black circles denote the streamwise velocity at Creek 2 high water. The low marsh elevation range as well as local Mean Higher High Water (MHHW) are indicated by grey and black horizontal lines, respectively. Subsequent analysis for the data use the following grouping: Neap tide (Tidal Amplitude < 0.8 m.a.s.l.), Intermediate tide (0.8 m.a.s.l. < Tidal Amplitude < 1.15 m.a.s.l.), and Spring tide (Tidal Amplitude > 1.15 m.a.s.l.).

4.1.1 Neap tides (Tidal Amplitude < 0.8 m.a.m.s.l.)

All creeks showed the characteristic stage-velocity curve whereby the flow gradually increased during flood tide (+ values), peaking as the marsh platform is overtopped and then decreasing after the floodable area expands (Boon, 1975; Healey et al., 1981; Mariotti & Fagherazzi, 2011). On average, the creek flood velocities peaked 60-70 min prior to high water, at 0.15 m/s, 0.20 m/s, and 0.30 m/s in each creek, respectively. At high water all creeks continued to inflow, albeit <0.05 m/s in Creeks 1 and 3 (<0.05 m/s). Creek 2 continued to inflow at 0.11 m/s, roughly 2 to 3 times faster than the other creeks. Creek 2 showed slack water 25 minutes after high water, and roughly 10 minutes following the other creeks. Peak ebb flow in Creek 1 occurred 92 minutes following high water, 30 minutes before Creeks 2 and 3.

4.1.2. Intermediate Tides (0.8 m.a.m.s.l. < Tidal Amplitude < 1.15 m.a.m.s.l.)

A different pattern among tidal creeks emerged between the Intermediate and Neap tides. In all creeks, the inflow gradually increased until the water level was between 0.72-0.82 m.a.s.m.l., or as the marsh platform flooded. However, for the remainder of the infilling period (1-2 hours) Creek 1 inflows rapidly diminished and were 0.02 m/s at high water. Creek 3 displayed peak inflow of 0.39 m/s, which was 2.1 times greater than at Creek 1 and 1.2 times greater than at Creek 2. Following the peak inflow, Creek 3 displayed the same diminishment of inflow (i.e., no inflow at high water) as did Creek 1. Conversely, Creek 2 displayed higher inflows (~0.10 m/s) and did not reverse until 26 minutes after high water. On average, Creek 2 flooded for ~40 minutes longer than Creeks 1 and 3 during the flood phase of the tide.

During the falling phase of the tide, flows began to increase and peaked when the water surface elevation was below the creekbanks, i.e., mostly channelized flow. Similar to the occurrence of peak flooding due to rapid expansion of floodable area, peak ebbing occurred when the excess platform water can only exit the system through the creeks (i.e., no overbank flows). Creek 2 peak ebb velocity was on average -0.86 m/s (1.4 times greater than Creek 1 and 1.6 times greater than Creek 2). Creek 2 peaked approximately 25 and 10 minutes after Creeks 1 and 3, respectively.

4.1.3. Spring Tides (Tidal Amplitude > 1.15 m.a.m.s.l.)

The most notable changes to stage-velocity patterns occurred during the spring tides. During these tides, the high water level exceeded the highest levees adjacent to Dean Creek, causing submergence in most, if not all, of the marsh in the study area. The flooding pattern for Creek 1 was essentially the same as it was for intermediate tides, with the same peak flood velocity. Both Creeks 2 and 3 increased in peak flood velocities by 14% and 5%, respectively. However, Creek 3 experienced slack water 65 minutes prior to high water, when the water level coincided with the highest levee elevations. As the water level continued to increase above the levee elevation, Creek 1 exhibited near-zero inflow and Creek 3 began to outflow. However, Creek 2 continued a sustained inflow (>0.15 m/s) until 30 minutes after high water (or as the water level began to recede). This phase lag caused a water level slope that drove a cross-marsh flow from Creek 2 to Creek 3.

As the water level fell below the elevation of the highest levees, the stage-velocity relationship in all creeks was similar to the patterns in Intermediate tides. The outflow was the highest in all creeks when the flow was fully channelized. On average, the peak outflow for each creek was 0.82, 0.65, and 1.01 m/s, respectively, representing increases of 32% for Creek 1, 25% for Creek 2, and 17% for Creek 3. With respect to the peak flood to ebb velocity ratio, all creeks showed stronger ebb currents than flood currents and are considered ‘ebb-dominated’.

4.2 Bottom and effective drag in intertidal creeks

4.2.1. Bottom Drag Estimated from ADVs

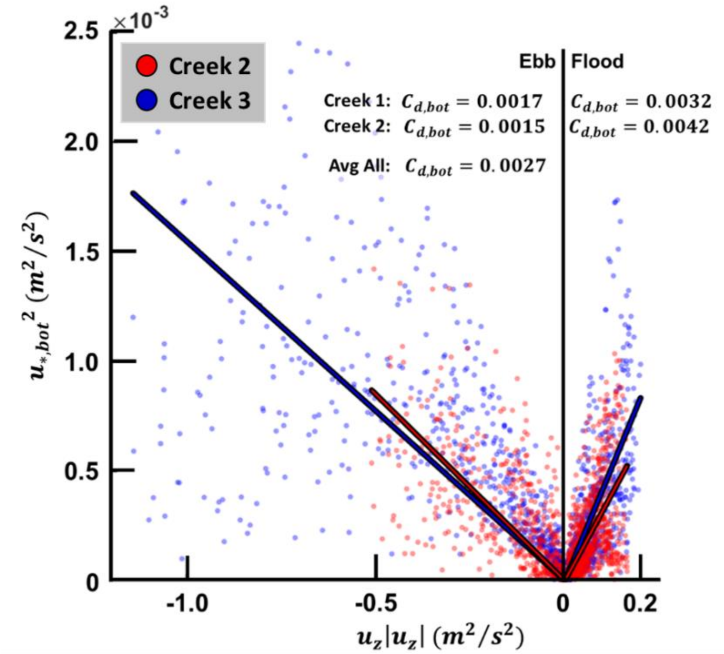

Figure 3. The balance between mean point-velocity measured (squared) at elevation z (x-axis) and the estimated shear velocity squared (y-axis) where the slope of the line represents the bed drag coefficient $C_{d,bot}$ shown for Creeks 2 and 3. The average of both creeks and phases is 0.0027.

In assessing the quadratic bottom drag coefficient throughout the 20 tide cycles in the dataset (Figure 3 A), for Creek 2 (red) it is 0.0032 ($R^2 = 0.35$) on the flood phase and 0.0017 ($R^2 = 0.45$) for the ebb phase. Similarly, the bottom drag in Creek 3 (blue) is 0.0042 ($R^2 = 0.58$) and 0.0015 ($R^2 = 0.54$) in the flood and ebb phases, respectively. Averaged across flood and ebb phases of all tides and across both creeks, the bottom drag is 0.0027 (SEM 6.40E-4) for $z = 0.30\,m$ above bed (canonical value = 0.0024). This value is comparable to that estimated by Voulgaris and Meyers (2004) of 0.0024 at $z = 0.15\,m$ above bed in a South Carolina, USA, salt marsh system located 300 km north of our study site with similar sediment and vegetation features. This drag estimate is used in subsequent estimates for velocity log-profile estimates, tidal discharge and ultimately TSS fluxes for the measured time period.

4.2.2. Stage Varying Effective Drag

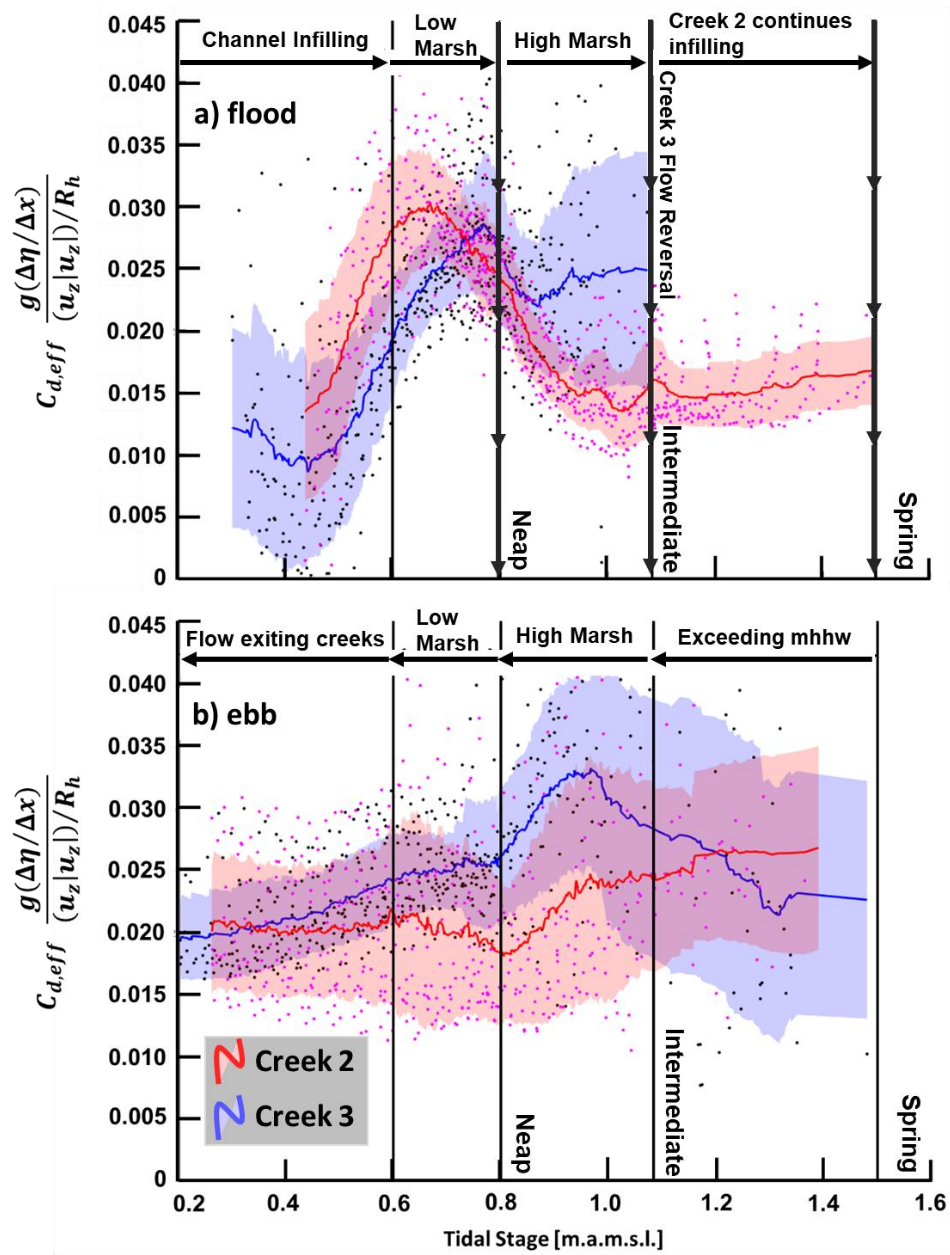

Figure 4. Effective drag (y-axis) plotted against tidal stage (x-axis) for Creeks 2 (red) and 3 (blue). The shaded area represents ±1 local standard deviation and the solid lines represent a moving average. Points indicate instantaneous values. Effective drag is separated by tidal stage such that panel (a) represents the flood, or rising limb, phase of the tide and panel (b) is the ebb, or falling limb of the tide. Single-headed arrows denote the direction to read the drag values over the course of a given tide, i.e. left to right for flood in panel (a), and right to left for ebb in panel b. In (a) a clear increase in drag occurs as the tidal stage increases with the flood tide, and reaches a maximum between 0.6-0.8 m.a.m.s.l. in each creek, when flows begin spreading across low and high marsh elevations. After this maximum, Creek 2 drag reduces by 50%. Because Creek 3 inflows approach zero during spring tides, the drag cannot be properly evaluated (the denominator goes to zero), as expressed by no blue Creek 3 line being expressed at high tidal stages on the right of panel (a).

The effective drag is a measure of how much driving or restoring force is needed to produce a resultant flow; in other words, how much friction is resisting the flow. Shallow tidal embayments have long been recognized as systems dominated by friction (Friedrichs & Madsen, 1992; LeBlond, 1978; Rinaldo et al., 1999). Tidal waves in these systems can be represented as quasi-steady diffusive waves, where the local and advective accelerations are much smaller than the pressure gradient and friction terms in the momentum balance (i.e., negligible terms on the left-hand side of Equation 7). Our measurements indicate that the pressure gradient and friction terms are both $O(10^{-3}\ to\ 10^{-2}$ m/s^2) in Creeks 2 and 3. These values are between 1 and 2 orders of magnitude higher than found by French and Stoddart (1992) and Healy et al. (1981) in their respective field studies of tidal channels.

Estimates of the effective drag coefficient (Fig. 4) ranged between 3 and 12 times greater than bed drag $(= 0.0027)$ in Creeks 2 and 3. During the early stages of the flooding tide (Figure 4a), there is a minimum drag in both creeks (=0.01-0.015). Equation 9 illustrates that when the water depth approaches zero, the hydraulic radius approaches zero, indicating that the total source of friction is from the bed. However, because of the 20-30 cm height of our instruments, we were unable to directly measure this portion of the flow as the instruments were no longer submerged. As the stage increased, the drag coefficient increased in both creeks and peaked at values of 0.03 and 0.028 for Creeks 2 and 3, respectively. These peaks occurred due to the expansion of floodable marsh area coinciding with the early stages of overmarsh flooding and the flood waters spreading across the platform (see average depth derived from Digital Elevation Model in supplemental Figure 7). These values occurred when the water level was between 0.6 and 0.8 m.a.m.s.l.

Following the maximum effective drag value, the drag declined in both creeks, corresponding to an average increase of water depth across the marsh as flood waters filled the marsh. In Creek 3, because inflow velocities sharply fall during spring tides (as explained above and shown in Fig. 2), the calculation for drag no longer yields realistic results (i.e. friction term becomes too small). This reduction of inflow (and early flow reversal) corresponded to a cross-marsh water surface gradient (from Creeks 1/2 to Creek 3; see Figure 6). Conversely, the drag in Creek 2 approached a near constant value of 0.015 for tidal stages above 1.15 m.a.m.s.l., corresponds to the m.h.h.w. and Dean Creek levee elevations. During the ebb phase (Figure 4b), for tidal stages greater than 0.8 m.a.m.s.l., there is increased uncertainty in the estimates for the drag due to variations in the water surface slope. However, both creeks converge to an effective drag of 0.020 when approaching 0.2 m.a.m.s.l. The effective drag estimates indicated that, over the duration of a tidal cycle, the drag from the landscape and vegetation effects is larger than bed drag. Furthermore, the magnitude of the effective drag suggests that the intertidal creeks can be treated as similar to steady-state systems, where the momentum balance is dominated by pressure gradient and friction terms.

4.3. Tidal transport and directionality in creeks

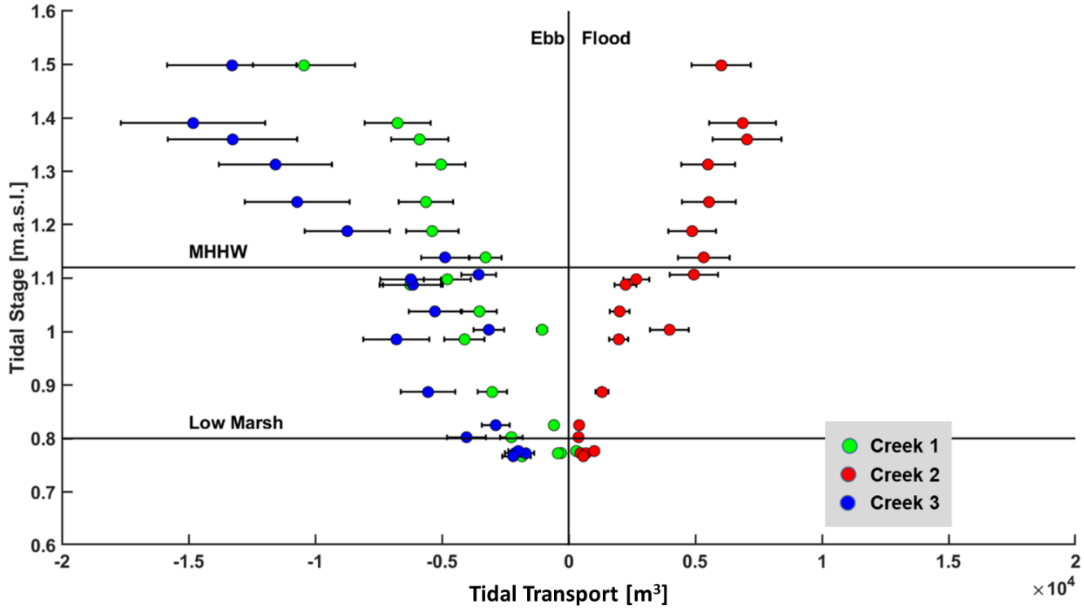

Figure 5. Estimated tidal transport in each tidal creek for each tide of measured data vs tidal amplitude. Note that for neap tides (amplitude <0.8), it is assumed that the exchange should be essentially zero, i.e. water entering an individual creek exits, however, the measurement period does not cover the entire tide.

Assessing tidal transport helps understanding and predicting the longer-term evolution of marshes as tidewaters exchange sediments and other suspended biological material between salt marshes and their surrounding estuaries. Our findings (Figure 5) indicated that during neap tides, the transport was essentially neutral, or the same flow entered and exited the same creek. During neap tides, most if not all of the water, has been found to be transported through the channel sections (Bayliss-Smith et al., 1979; Bouma et al., 2005; Fagherazzi et al., 2008b). However, for intermediate and spring tides, our estimates indicate that Creeks 1 and 3 have net outflows (negative tidal transports), whereas Creek 2 shows net inflow. In order to have a net transport, more water needs to exit the creek section rather than enter, or vice versa. This suggests an overmarsh circulation which is further supported by the measured cross-marsh water-surface gradients. Torres et al. (2007) measured flow with velocimeters near the heads of tidal creeks and found regular exchanges of water between two nearby creeks. They suggested that drainage divides on the marsh may not be as apparent when compared to fluvial systems where they are well defined. Our measurements complement their findings. A consequence of this imbalance may be indicated by our TSS transport estimates for one tidal cycle. Creek 1 was net exporting and Creeks 2 and 3 were net importing (Figure 8 - supplement). Differential transport of sediments on the landscape suggest a potential for heterogeneous vertical accretion, whereby the marsh may be increasing or decreasing elevation differently with a given marsh drainage area.

Tidal-asymmetry models have been developed to explain why creeks and channels experience differing discharges (velocities) at the same stage for different phases of the tide. Initially Boon (1975) developed a model stating that the cross-section discharge q is given by:

$$q = A\,\frac{dh}{dt} \tag{10}$$

where A is the free surface area inside the section, and h is the tidal stage with time dependence t. However, this model is unable to capture the difference in elevation for flood and ebb peaks as the change in tidal stage $\frac{dh}{dt}$ was considered symmetric for both flood and ebb. Subsequent field studies identified the need to incorporate other factors such as overbank flow, wind stress, and account for friction on the marsh platform. Fagherazzi et al. (2008a) further improved Boon's model by incorporating geomorphic features on the landscape (i.e. friction), allowing time-varying infilling of the marsh, and incorporating overbank flow. Of note is the estimation for water surface gradients based on Rinaldo et al. (1999) which is solved for using the following Poisson equation:

$$\nabla_{\eta}^{2} = \frac{\Lambda}{z_0^2}\frac{\partial \eta_0}{\partial t} \tag{11}$$

Where ∇_{η}^{2} is the water surface gradient, Λ is a friction coefficient, η_0 is the tidal stage at the inlet, and z_0 is the average water elevation in the marsh. They noted that this formulation will yield identical results for flowpaths during the flood and ebb as $\frac{\partial \eta_0}{\partial t}$ yields the same value between flood and ebb. For our field study, a marsh with an upland terrestrial boundary, this assumption does not hold as the along channel gradients do not scale linearly with $\frac{\partial \eta_0}{\partial t}$ (differing drag effects between flood and ebb tides; see Figure 4) and circulation occurs during both intermediate and spring tides.

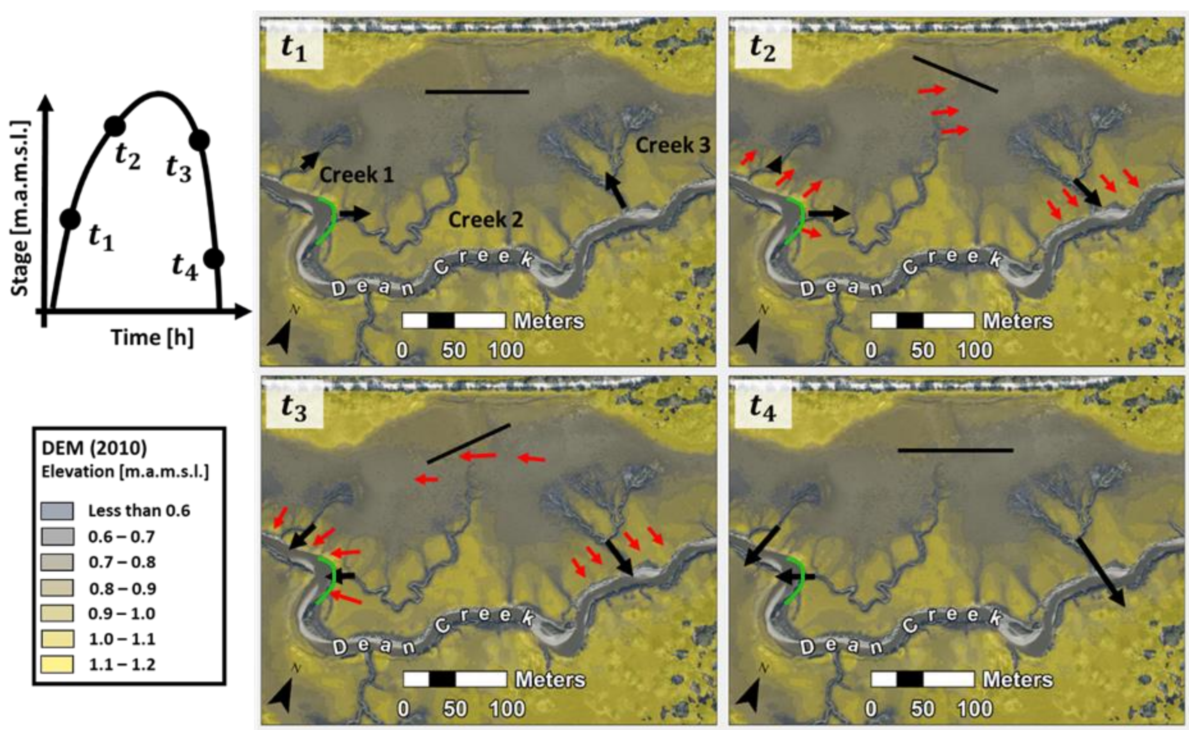

Figure 6. (a) Tidal stage during a representative intermediate or spring tide. Black arrows represent along-creek velocities and red arrows represent overbank or marsh platform flow directions. The green arc is the outer bend of Dean Creek referred to in Section 4.4. At timepoint t1), the water flows through the tidal creeks and there is not a clear cross marsh water surface gradient (denoted by black horizontal bar). Later in the flood, a cross marsh gradient (from direction of Creek 1/2 to Creek 3) developed and overbank flow began (t2). At this time, Creek 3 began outflowing following high water, the cross marsh gradient reversed, and all creeks outflowed (t3). Overbank outflow occurred at this time as well. As the water stage fell further, the flow was only concentrated in the tidal creeks (t4). During timepoint t2, we suggest Creek 2 may have sustained inflows due to Dean Creek outer bend super elevation. At timepoint t3, the bend super elevation would suppress the outflow of Creek 2.

4.4 Role of tidal meander in altering creek and marsh flow

While there were no measurements of flow along Dean Creek, data at the smaller creeks suggest that Dean Creek may alter the stage-velocity relationships, and ultimately drive creek-to-creek flow interactions and overmarsh circulation. Figure 6 illustrates the relative magnitude of velocity in each creek, the cross-marsh gradient direction, and presence of overbank flow for different times during an intermediate or spring tide. Torres et al. (2007) presented an idealized representation of flooding in their system, where in early stages of flood the water propagates along the tidal channels. Following their proposition (or portrayal), overbank flow begins as the channel levees are overtopped subsequently driving a circulation linked to the water-level slopes. This marsh follows a consistent pattern. However, the pattern is insufficient to explain the 'shorting' of the inflow in Creek 1, seaward of Creek 2, which continued to display inflow beyond high water.

A potential mechanism inflow 'shorting' at Creek 1 and continued and sustained inflow at Creek 2 could be a super-elevation at an outer bend on Dean Creek (highlighted in green in Figure 6). Bend super elevations, or a lateral setup on the outer bend and set-down on the inner bend of a meander, develop through centrifugal accelerations (e.g. (Blanckaert & De Vriend, 2003; Dietrich & Smith, 1983; Seminara, 2006) . When water flows around bends centrifugal force redistributes momentum laterally across the channel. This causes an imbalance in pressure gradient that drives a secondary flow consisting of surface flow toward the outer bend and near-bed flow toward the inner bend (Blanckaert & De Vriend, 2003; Dietrich & Smith, 1983; Seminara, 2006). Recently, Kranenberg et al. (2019) measured tidal meander bend super elevations in a New England salt marsh in a weakly stratified tidal channel ($\frac{Channel\ Width}{Radius\ of\ Curvature} = 0.7$ in their study, our study $\frac{Channel\ Width}{Radius\ of\ Curvature} = 0.8$ at confluence of Dean Creek and Creek 2). During maximum flood and ebb of a spring tide, they measured a ~3 cm cross-channel setup. During flood, the outer bend water surface elevation was found to be 0.1 cm lower than the upstream location whereas the downstream segment (of approximately similar length) was 2.4 cm lower in elevation than the apex. Between Creeks 1 and 2, we measured an along channel (Dean Creek) water surface anomaly of 1-2 cm (Creek 2 higher than Creek 1) during the flooding phase (not shown). This finding was contradictory to our initial expectation that Creek 1 would consistently exhibit higher water surface elevations during the flood phase as a result of its closer proximity to channel outlet to Doboy Sound relative to Creek 2. Furthermore, at peak ebb, Kranenberg et al. (2019) found that the outer bend water surface elevation was 0.8 and 3.4 cm higher than the upstream and downstream locations. This may provide insight as to why Creek 2 has a suppressed peak outflow when compared to Creeks 1 and 3 (26% less than Creek 1 and 55% less than Creek 3), as the bend super-elevation has the potential to suppress the allowable along-channel water surface gradient during ebb.

5. Conclusions

Our field measurements of flow in three small intertidal creeks over a spring-neap period revealed opposing tidal asymmetries within a confined drainage area. We provide estimates of effective drag coefficients for small intertidal creeks, which exhibited similar magnitudes as found in sea grass beds and coral reefs. Furthermore, our measurements indicate regular exchanges of water between creeks and overmarsh circulation, similar to what was found in Torres et al. (2007). We suggest that main channel flow patterns (such as meander bend super-elevations) may have a stronger effect on tidal creek asymmetries than previously recognized. Our findings also suggest that significant heterogeneity in the delivery of suspended sediments and biological material may be driven by the creek-creek divergences in flow and sediment transport, and cross-marsh circulation. We do not have direct measurements of sediment deposition rates or larval delivery, to quantify this heterogeneity. However, our observations of populations of filter-feeding mussels (*Geukensia demissa*) at the creekhead of Creek 2/3 are more than an order of magnitude higher compared to Creek 1 indicate that faunal populations may be mediated by the exchanges that we document herein. We hypothesize that tidal asymmetries and cross-marsh circulations may interact with faunal populations to control patterns in salt marsh vertical accretion via sedimentation and ultimately the geospatial evolution of these biogenic landforms in response to sea-level rise (Angelini et al., 2016; Crotty et al., 2020; Crotty & Angelini, 2020).

Acknowledgments, Samples, and Data

Funding to support this research was provided by the UF Graduate Student Preeminence Award to CO, NSF CAREER (CBET #1652628) and NSF LTER (BIO-OCE #1832178) awards to CA; and OCE-1736830 to AVL. Field activities were supported by the Sapelo Island NERR and the GCE-LTER staff. We would like to thank Dr. Alex Sheremet for providing instruments to support this work. Comments from the Angelini Lab, Dr. Thomas Bianchi, Dr. Elise Morrison, and Dr. Rocky Geyer improved the intellectual merit and rigor of this manuscript. Data for this work are in the process of being uploaded to the Georgia Coastal Ecosystems LTER database hosted at http://gce-lter.marsci.uga.edu/.

References

Angelini, C., Griffin, J. N., Van De Koppel, J., Lamers, L. P. M., Smolders, A. J. P., Derksen-Hooijberg, M., et al. (2016). A keystone mutualism underpins resilience of a coastal ecosystem to drought. *Nature Communications*, *7*, 1–8. https://doi.org/10.1038/ncomms12473

Barbier, E., Hacker, S., Kennedy, C., Koch, E., Stier, A., & Silliman, B. (2011). The value of estuarine and coastal ecosystem services. *Ecological Monographs*, *81(2)*(2), 169–193.

Bayliss-Smith, T. P., Healey, R., Lailey, R., Spencer, T., & Stoddart, D. R. (1979). Tidal flows in salt marsh creeks. *Estuarine and Coastal Marine Science*, *9*(3), 235–255. https://doi.org/10.1016/0302-3524(79)90038-0

Blanckaert, K., & De Vriend, H. J. (2003). Nonlinear modeling of mean flow redistribution in curved open channels. *Water Resources Research*, *39*(12), 1–14. https://doi.org/10.1029/2003WR002068

Blanton, B. O., Werner, F. E., Seim, H. E., Luettich, R. A., Lynch, D. R., Smith, K. W., et al. (2004). Barotropic tides in the South Atlantic Bight. *Journal of Geophysical Research C: Oceans*, *109*(12), 1–17. https://doi.org/10.1029/2004JC002455

Bo, T., & Ralston, D. K. (2020). Flow Separation and Increased Drag Coefficient in Estuarine Channels With Curvature. *Journal of Geophysical Research: Oceans*, *125*(10), 1–25. https://doi.org/10.1029/2020JC016267

Boon, J. D. (1975). Tidal discharge asymmetry in a salt marsh drainage system,. *Limnology and Oceanography*, *20*(1), 71–80. https://doi.org/10.4319/lo.1975.20.1.0071

Bouma, T J, Govers, G., Lauwaet, D., & Temmerman, S. (2005). Flow paths of water and sediment in a tidal marsh: Relations with marsh developmental stage and tidal inundation height. *Estuaries*, *28*(3), 338–352. https://doi.org/10.1007/BF02693917

Bouma, Tjeerd J., van Belzen, J., Balke, T., Zhu, Z., Airoldi, L., Blight, A. J., et al. (2014). Identifying knowledge gaps hampering application of intertidal habitats in coastal protection: Opportunities & steps to take. *Coastal Engineering*, *87*, 147–157. https://doi.org/10.1016/j.coastaleng.2013.11.014

Christiansen, T., Wiberg, P. L., & Milligan, T. G. (2000). Flow and sediment transport on a tidal salt marsh surface. *Estuarine, Coastal and Shelf Science*, *50*(3), 315–331. https://doi.org/10.1006/ecss.2000.0548

Coverdale, T. C., Altieri, A. H., Bertness, M. D., & Kotanen, P. M. (2012). Belowground herbivory increases vulnerability of New England salt marshes to die-off. *Ecology*, *93*(9), 2085–2094. https://doi.org/10.1890/12-0010.1

Crotty, S. M., & Angelini, C. (2020). Geomorphology and Species Interactions Control Facilitation Cascades in a Salt Marsh Ecosystem. *Current Biology*, *30*(8), 1562-1571.e4. https://doi.org/10.1016/j.cub.2020.02.031

Crotty, S. M., Ortals, C., Pettengill, T. M., Shi, L., & Olabarrieta, M. (2020). Sea-level rise and the emergence of a keystone grazer alter the geomorphic evolution and ecology of southeast US salt marshes. https://doi.org/10.1073/pnas.1917869117

Dietrich, W. E., & Smith, J. D. (1983). Influence of the point bar on flow through curved channels. *Water Resources Research*, *19*(5), 1173–1192. https://doi.org/https://doi.org/10.1029/WR019i005p01173

Dyer, K. R. (1971). Current Velocity Profiles in a Tidal Channel. *Geophysical Journal of the Royal Astronomical Society*, *22*(2), 153–161. https://doi.org/10.1111/j.1365-246X.1971.tb03589.x

Fagherazzi, S., Hannion, M., & D'Odorico, P. (2008a). Geomorphic structure of tidal hydrodynamics in salt marsh creeks. *Water Resources Research*, *44*(2), 1–12. https://doi.org/10.1029/2007WR006289

Fagherazzi, S., Hannion, M., & D'Odorico, P. (2008b). Geomorphic structure of tidal hydrodynamics in salt marsh creeks. *Water Resources Research*, *44*(2), 1–12. https://doi.org/10.1029/2007WR006289

Fagherazzi, S., Kirwan, M. L., Mudd, S. M., Guntenspergen, G. R., Temmerman, S., D'Alpaos, A., et al. (2012). Numerical models of salt marsh evolution: Ecological, geomorphic, and climatic factors. *Reviews of Geophysics*, *50*(1), 1–28. https://doi.org/10.1029/2011RG000359

Feddersen, F., Gallagher, E. L., Guza, R. T., & Elgar, S. (2003). The drag coefficient, bottom roughness, and wave-breaking in the nearshore. *Coastal Engineering*, *48*(3), 189–195. https://doi.org/10.1016/S0378-3839(03)00026-7

French, J. R., & Stoddart, D. R. (1992). Hydrodynamics of salt marsh creek systems: Implications for marsh morphological development and material exchange. *Earth Surface Processes and Landforms*, *17*(3), 235–252. https://doi.org/10.1002/esp.3290170304

Friedrichs, C. T., & Madsen, O. S. (1992). Nonlinear diffusion of the tidal signal in frictionally dominated embayments. *Journal of Geophysical Research*, *97*(C4), 5637. https://doi.org/10.1029/92jc00354

Goring, D. G., & Nikora, V. I. (2002). Despiking acoustic doppler velocimeter data. *Journal of Hydraulic Engineering*, *128*(1), 117–126. https://doi.org/10.1061/(ASCE)0733-9429(2002)128:1(117)

Grant, W. D., & Madsen, O. S. (1982). Movable bed roughness in unsteady oscillatory flow. *Journal of Geophysical Research: Oceans*, *87*(C1), 469–481. https://doi.org/10.1029/JC087iC01p00469

Healey, R. G., Pye, K., Stoddart, D. R., & Bayliss-Smith, T. P. (1981). Velocity variations in salt marsh creeks, Norfolk, England. *Estuarine, Coastal and Shelf Science*, *13*(5), 535–545. https://doi.org/10.1016/S0302-3524(81)80056-4

Hughes, Z. J. (2012). Tidal Channels on Tidal Flats and Marshes BT - Principles of Tidal Sedimentology. In R. A. Davis Jr. & R. W. Dalrymple (Eds.) (pp. 269–300). Dordrecht: Springer Netherlands. https://doi.org/10.1007/978-94-007-0123-6_11

Kranenburg, W. M., Geyer, W. R., Garcia, A. M. P., & Ralston, D. K. (2019). Reversed lateral circulation in a sharp estuarine bend with weak stratification. *Journal of Physical Oceanography*, *49*(6), 1619–1637.

https://doi.org/10.1175/JPO-D-18-0175.1

LeBlond, P. H. (1978). On tidal propagation in shallow rivers. *Journal of Geophysical Research*, *83*(C9), 4717. https://doi.org/10.1029/jc083ic09p04717

Li, C., Valle-Levinson, A., Atkinson, L. P., Wong, K. C., & Lwiza, K. M. M. (2004). Estimation of drag coefficient in James River estuary using tidal velocity data from a vessel-towed ADCP. *Journal of Geophysical Research: Oceans*, *109*(3), 1–11. https://doi.org/10.1029/2003jc001991

Lin, Q., & Mendelssohn, I. A. (2012). Impacts and recovery of the deepwater horizon oil spill on vegetation structure and function of coastal salt marshes in the northern gulf of Mexico. *Environmental Science and Technology*, *46*(7), 3737–3743. https://doi.org/10.1021/es203552p

Mariotti, G., & Fagherazzi, S. (2011). Asymmetric fluxes of water and sediments in a mesotidal mudflat channel. *Continental Shelf Research*, *31*(1), 23–36. https://doi.org/10.1016/j.csr.2010.10.014

Monismith, S. G. (2007). Hydrodynamics of coral reefs. *Annual Review of Fluid Mechanics*, *39*, 37–55. https://doi.org/10.1146/annurev.fluid.38.050304.092125

Monismith, S. G., Hirsh, H., Batista, N., Francis, H., Egan, G., & Dunbar, R. B. (2019). Flow and Drag in a Seagrass Bed. *Journal of Geophysical Research: Oceans*, *124*(3), 2153–2163. https://doi.org/10.1029/2018JC014862

Nepf, H. M. (1999). Drag, turbulence, and diffusion in flow through emergent vegetation. *Water Resources Research*, *35*(2), 479–489. https://doi.org/10.1029/1998WR900069

Nidzieko, N. J., & Ralston, D. K. (2012). Tidal asymmetry and velocity skew over tidal flats and shallow channels within a macrotidal river delta. *Journal of Geophysical Research: Oceans*, *117*(3), 1–17. https://doi.org/10.1029/2011JC007384

Nikuradse, J. (VDI V. (1933). Strömungsgesetze in rauhen Rohren.

Pieterse, A., Puleo, J. A., Mckenna, T. E., & Figlus, J. (2012). Estuarine , Coastal and Shelf Science In situ measurements of shear stress , erosion and deposition in man- made tidal channels within a tidal saltmarsh. *Estuarine, Coastal and Shelf Science*, *192*(2017), 29–41. https://doi.org/10.1016/j.ecss.2017.04.028

Pieterse, A., Puleo, J. A., Mckenna, T. E., & Aiken, R. A. (2015). Near-bed shear stress, turbulence production and dissipation in a shallow and narrow tidal channel. *Earth Surface Processes and Landforms*, *40*(15), 2059–2070. https://doi.org/10.1002/esp.3782

Rantz, S. E. (1982). *Measurement and computation of streamflow*. *Water Supply Paper* (Vol. 1 & 2). https://doi.org/10.3133/wsp2175

Rennie, C. D., & Hay, A. (2010). Reynolds Stress Estimates in a Tidal Channel from Phase-Wrapped ADV Data. *Journal of Coastal Research*, *261*(261), 157–166. https://doi.org/10.2112/08-1090.1

Rinaldo, A., Fagherazzi, S., Lanzoni, S., Marani, M., & Dietrich, W. E. (1999). Tidal networks: 2. Watershed delineation and comparative network morphology. *Water Resources Research*, *35*(12), 3905–3917. https://doi.org/10.1029/1999WR900237

Rusello, P. (2009). A practical primer for pulse coherent instruments. *Nortek Technical Note No.: TN-027*, 1–17. Retrieved from http://scholar.google.com/scholar?hl=en&btnG=Search&q=intitle:A+Practical+Primer+for+Pulse+Coherent+Instruments#0

Seminara, G. (2006). Meanders. *Journal of Fluid Mechanics*, *554*, 271–297. https://doi.org/10.1017/S0022112006008925

Soulsby, R. L. (1983). Chapter 5 The Bottom Boundary Layer of Shelf Seas. In B. B. T.-E. O. S. Johns (Ed.), *Physical Oceanography of Coastal and Shelf Seas* (Vol. 35, pp. 189–266). Elsevier. https://doi.org/https://doi.org/10.1016/S0422-9894(08)70503-8

Struyf, E., Temmerman, S., Fagherazzi, S., Wiberg, P. L., Raymond, P. A., & Zhao, Y. (2013). Fluxes of water, sediments, and biogeochemical compounds in salt marshes. *Ecological Processes*, *2*(1), 1–16. https://doi.org/10.1186/2192-1709-2-3

Sullivan, J. C., Torres, R., & Garrett, A. (2019). Intertidal Creeks and Overmarsh Circulation in a Small Salt Marsh Basin. *Journal of Geophysical Research: Earth Surface*, *124*(2), 447–463. https://doi.org/10.1029/2018JF004861

Temmerman, S., Bouma, T. J., Govers, G., & Lauwaet, D. (2005). Flow paths of water and sediment in a tidal marsh: Relations with marsh developmental stage and tidal inundation height. *Estuaries*, *28*(3), 338–352. https://doi.org/10.1007/BF02693917

Temmerman, Stijn, Meire, P., Bouma, T. J., Herman, P. M. J., Ysebaert, T., & De Vriend, H. J. (2013). Ecosystem-based coastal defence in the face of global change. *Nature*, *504*(7478), 79–83. https://doi.org/10.1038/nature12859

Torres, R., & Styles, R. (2007). Effects of topographic structure on salt marsh currents. *Journal of Geophysical Research: Earth Surface*, *112*(2), 1–14. https://doi.org/10.1029/2006JF000508

Voulgaris, G., & Meyers, S. T. (2004). Temporal variability of hydrodynamics, sediment concentration and sediment settling velocity in a tidal creek. *Continental Shelf Research*, *24*(15), 1659–1683. https://doi.org/10.1016/j.csr.2004.05.006

Voulgaris, G., & Trowbridge, J. (1998). Evaluation of the Acoustic Doppler Velocimeter (ADV) for Turbulence Measurements*. *Journal of Atmospheric and Oceanic Technology*, *15*(1), 272–289. https://doi.org/10.1175/1520-0426(1998)015<0272:eotadv>2.0.co;2

Walker, J. F. (1988). GENERAL TWO-POINT METHOD FOR DETERMINING VELOCITY IN OPEN CHANNEL. *Journal of Hydraulic Engineering*, *114*(7), 801–805. Retrieved from http://pubs.er.usgs.gov/publication/70013659

Warner, S. J. (Oregon S. U., & MacCready, P. (University of W. (2014). Journal of Geophysical Research : Oceans headland : Internal waves versus eddies. *Journal of Geophysical Research C: Oceans*, 1554–1571. https://doi.org/10.1002/2013JC009757.Received

Yen, B. C. (2002). Open Channel Flow Resistance. *Journal of Hydraulic Engineering*, *128*(1), 20–39. https://doi.org/10.1061/(asce)0733-9429(2002)128:1(20)